

Generation and precise control of dynamic biochemical gradients for cellular assays

Yasushi Saka,* Murray MacPherson, and Claudiu V. Giuraniuc

School of Medicine, Medical Sciences & Nutrition, Institute of Medical Sciences, University of Aberdeen, Foresterhill, Aberdeen AB25 2ZD, United Kingdom

E-mail: y.saka@abdn.ac.uk

Abstract

Spatial gradients of diffusible signalling molecules play crucial roles in controlling diverse cellular behaviour such as cell differentiation, tissue patterning and chemotaxis. Here we present a microfluidic platform for cellular assays that can generate and control diffusion-based gradients dynamically. A unique design of the device eliminates cross-flow between the source and sink channels, thereby stabilising gradients by passive diffusion. The platform also enables quick and flexible control of chemical concentration that makes highly dynamic gradients in diffusion chambers. Budding yeast cells cultured in a gradient of a chemical inducer expressed a reporter fluorescence protein in a concentration-dependent manner. This microfluidic platform serves as a versatile prototype applicable to a broad range of biomedical investigations.

*To whom correspondence should be addressed

Introduction

Biochemical gradients are ubiquitous in biological systems. Gradients convey spatial and temporal information and function as cues for cellular decisions such as differentiation, proliferation and chemotaxis. Knowing how cells respond to them is thus fundamentally important to biomedicine and biotechnology applications. A well-studied example of biochemical gradients is that of morphogens that pattern embryonic tissues in a concentration-dependent manner (reviewed in^{1–4}). Recent experimental evidence has suggested that the response of cells to morphogen gradients is regulated dynamically as the gradients change over time.^{2,4} Dynamics of morphogen gradients are therefore crucial for tissue patterning, as corroborated by our theoretical study.⁵ As biochemical gradients *in vivo* may never be static, investigations of cellular response to gradients require experimental means to control gradients in a dynamic manner to reproduce a natural cellular environment.

Microfluidic devices are becoming popular for studying gradients as they can generate and maintain desired gradient profiles stably for a long period.^{6–8} A number of different designs of microfluidic gradient generators have been proposed, which can be grouped into two categories:⁸ flow-based^{9–13} and diffusion-based gradient generators.^{14–24} The flow-based gradient is established by the diffusion at the interface of laminar flows. Diffusion-based designs utilise a passive diffusion between a source and a sink flow channel or reservoir of chemicals, which generates a linear gradient at steady states. Their advantages and disadvantages have previously been discussed.^{7,8} For example, flow-based designs, unlike diffusion-based ones, can generate gradients of complex profile and maintain them stably for a prolonged time. The method of creating such non-linear gradients can reveal unexpected cell behaviour, for instance, in neutrophil chemotaxis.^{10,25}

One of the major drawbacks of the flow-based gradient generators for cellular assays is that cell-to-cell communication by diffusible factors is disrupted by continuous flow as such factors are washed away. Cells also experience a flow-induced shear stress, which may affect cell behaviour. Diffusion-based designs can overcome these problems and are appropriate for

analysing the cell's response to gradients where autocrine or paracrine cell signaling plays an important role. A typical diffusion based design features rectangular chambers between a source and a sink flow channel. In devices with such a design,^{17,26} a technical difficulty is to minimize the unwanted cross-flow between the source and the sink to maintain a stable gradient.²² Different schemes have been proposed to rectify this problem of flow-induced perturbation: membranes,^{14,19} hydrogels¹⁶ or micropillars^{18,21} between channels and a diffusion chamber; microfluidic "jets" that inject small amounts of fluid with minimal flow over cells;¹⁵ increased flow resistance across the chamber by reducing its height;¹⁸ embedding cells in a collagen matrix;^{18,26} a two-layered device with micro-channels in the top layer and a buried diffusion chamber in the bottom layer.²⁷

Another notable solution for this technical challenge was put forward recently by Frank and Tay.²² In their flow-switching device, only one side of the chamber is exposed to the flow channels at a time. By alternate switching of the on-chip membrane valves separating the chamber and the source/sink channels, gradients were established while a cross flow in the chamber was eliminated. Its capability of generating extremely stable spatial gradients was demonstrated with molecules such as lipopolysaccharides (LPS), tumour necrosis factor- α (TNF- α) and platelet-derived growth factors (PDGF) along with a fluorescent tracer (FITC-dextran, 40 kDa).²²

The reliable maintenance of gradients by the flow-switching scheme, however, depends on the size of diffusing molecules (i.e. diffusion coefficients), the length of a chamber and the duration between valve switching, as gradients degrade by diffusion in a closed chamber. Our calculation suggests that in a chamber of 1 mm length with 60 seconds between flow-switching (as specified in²²), molecular weights need to be larger than \sim 3.5 kDa (see Supplementary Information); many biologically active molecules fall below this threshold. Microfluidic gradient devices for unicellular organisms like yeast or *Dictyostelium* usually have diffusion chambers of less than 1 mm in length (for example^{17,20}). In a shorter chamber of 500 μ m, it may not be possible to maintain gradients of any biochemicals reliably with the

flow-switching scheme (Supplementary Information) unless using a shorter period of switching cycles. The interval of flow-switching could be shortened in the flow-switching device for fast-diffusing (low molecular weight) molecules. Yet, it makes it necessary to reduce the number of parallel gradients that can be controlled in a single chip, compromising one of the very advantages of its design.

In this paper we demonstrate a device with an alternative design for diffusion-based gradient generation. Our design has a channel junction upstream of the diffusion chambers, where the source and sink flows are merged to create a laminar flow away from the cell chambers; this enables precise balancing of flows in the source and sink channels thereby eliminating cross flows in the chambers. A similar idea was adopted in the device developed by Atencia *et al.*;²⁷ their device also merges the source and sink flows separated by a laminar interface in the upper layer, which in turn generate a gradient in the chamber in the bottom layer. In their device, however, there is a diffusive mixing between the merged streams, which may be an issue depending on the length of the laminar interface and the flow rates. To avoid a diffusive mixing, our device has a thin separation wall that splits the merged source/sink flows towards the cell chambers. Our device has also adopted the design features reported previously including chaotic mixer channels²⁸ with the so-called Dial-A-Wave (DAW) junction.²⁹ These features allow rapid and independent control of biochemical concentration in the source/sink flows.

We demonstrate the capability of our device using fluorescent tracer dyes and yeast cells harbouring a fluorescent protein reporter gene that are exposed to a gradient of the inducer doxycycline (Dox). Unlike the flow-switching device, our design allows stable gradient generation irrespective of the molecular mass, as well as a rapid and dynamic control of gradients.

Materials and Methods

Microfluidic device fabrication

The microfluidic devices were fabricated using conventional soft-lithography methods with poly(dimethylsiloxane) (PDMS).³⁰ Silicon wafers (10 cm diameter) patterned with SU8 photoresist were custom-ordered from Kelvin Nanotechnology Ltd. (Glasgow, UK). AutoCAD (Autodesk) was used to draw the device design. CAD files are available on request. Device chips were made by pouring PDMS (Sylgard 184, Dow Corning; 10:1 mix with curing agent) over the mold. PDMS was then degassed, cured at 70°C for 3 hours, peeled from the mold and cut into individual chips. Holes for media inlets and outlets were punched through the chip using a sharpened Harris UNI-CORE™ biopsy punch (0.5 mm). Dust was removed from PDMS chips and coverslips by ionizing air (nitrogen) gun (Top Gun, Simco) before assembly. PDMS chips and coverslips were bonded together after treatment with a plasma cleaner (Zepto ONE, Diener Electronic; HF generator 50 % (~15 W), 30 seconds). Assembled chips were then cured further at 60 °C overnight. Microbore tubing (ID/OD 0.02"/0.06"; Cole-Parmer, Tygon S-54-L) was used to connect a PDMS chip and media reservoir syringes. Hydrostatic pressure actuators are fabricated according to Ferry et al.,²⁹ which is controlled by a Raspberry Pi computer (Raspberry Pi 2 Model B); <https://www.raspberrypi.org>) and driven by a Java code modified from²⁹ (<http://biodynamics.ucsd.edu/dialawave/>). The Java source code is available upon request. Setup and operation protocol of the platform is described in detail in Supplementary Information.

Yeast strains and media

Two diploid strains of yeast *S. cerevisiae* MM169 and MM201 were used in this study, each of which harbours a fluorescent protein reporter gene (destabilised version of yVenus,³¹ an enhanced YFP). MM169 also has a gene encoding the transcriptional activator rtTA of the Tet-On system³¹ while MM201 has a tandem array of genes encoding rtTA and TetR-Ssn6 (a

synthetic transcriptional repressor) that constitutes the activator/repressor dual system.³² See Supplementary Information for the illustration of these gene constructs (Supplementary Information; Fig. S4A for MM169; Fig. S4C for MM201), which were all integrated in the genome. Details of the construction of these strains will be described elsewhere. For microfluidics experiments, yeast cells were first grown overnight at 30 °C in 10 ml synthetic complete media with raffinose (SMR), the composition of which is identical to the synthetic complete (SC) media³³ except glucose is replaced with raffinose (2 %; Formedium, cat. no. RAF01). On the following day the SMR cell culture was spun down at 3,000 g for 10 min and resuspended in 2 ml synthetic complete media with maltose (SMM; same as SC with maltose (2 %; BD Difco cat. no. 216830) replacing glucose) supplemented with BSA (Sigma A7906; final concentration at 0.01 %). Cells were then injected into a microfluidic device by 20 ml syringe through 10 cm of Tygon tube connected to the waste port. Cell loading procedure is detailed in Supplementary Information. Once cells were loaded in the device, SMM was used for cell growth. Doxycycline was added to one of the reservoir media to the final concentration of 2 μ g/ml. For shake flask experiments (Supplementary Information Fig. S4) yeast strains were cultured in 10 ml of SMR at 30 °C overnight. These precultures were then diluted to $OD_{600} = 0.4$ in 10 ml SC, SMR or SMM and continued to be grown at 30 °C. Each cell culture was split after 2 hours and either treated with doxycycline (Dox) (at the final concentration as indicated in Fig. S4) or left untreated. After further 7 hours culture at 30 °C, images were captured by fluorescence microscopy using the same imaging system for microfluidics experiments.

Microscopy and data analysis

Fluorescent tracer molecules were used at the following final concentrations in SC or SMR media: Cascade Blue hydrazide (CB; Trilithium salt, Thermo-Fisher) at 20 μ M, Sulforhodamine 101 (SR; Sigma-Aldrich S7635) at 10 μ g/ml and Fluorescein-dextran (FD; molecular weight 10,000, Sigma-Aldrich FD10S) at 1 mg/ml. For microfluidic experiments with yeast

cells, CB was added to SMM. For microscopy we used a Zeiss Axio Observer Z1 microscope equipped with an incubation chamber, CCD camera (Coolsnap HQ2, Photometrics) and Axiovision software (v4.8.2 SP3 (08-2013)). Either 20x (Ph2) or 40x (Ph3) objective was used for imaging. Fluorescence images were captured using Zeiss 62 HE BFP/GFP/HcRed filter set (excitation filter: BP370/40 for CB; BP474/28 for FD and Venus; BP585/35 for SR).

To quantify the gradients of fluorescent tracers, a rectangular region (width = 100 μm) in the captured images corresponding to a single diffusion chamber was cropped using ImageJ (version 1.50g). Average (total) pixel intensities were calculated along each single pixel line parallel to the main flow channels (orthogonal to the direction of diffusion). Fluorescence intensities in the main flow channels are represented by the intensity of a single pixel line parallel to the flows, approximately 20 μm away from the diffusion chamber's edge. Theoretical calculations of channel flows and diffusion/adsorption models were performed using Mathematica software (version 10.4, Wolfram Research). For details of the models, see Supplementary Information.

Results and Discussion

Device design

The design is based on the devices developed by Paliwal et al.¹⁷ and Ferry et al.²⁹ The microfluidics device consists of main channels, a pair of mixer modules and rectangular diffusion/cell chambers (Fig. 1). Flows in the chip are controlled by hydrostatic pressure. A single unit of the controller holds two media reservoirs that are connected to a pair of inlet ports (M1-M2 or M3-M4 in Fig. 1A). Media inputs from these ports flow through a "Dial-A-Wave" (DAW) junction²⁹ (Fig. 1A and B). At the DAW junction two media inputs are combined and mixed while passing through a staggered herringbone mixer (SHM) channel²⁸ (Fig. 1A (highlighted in green) and C). The mixing ratio is controlled precisely by

the hydrostatic pressure controller adopted from Ferry et al.²⁹ (Fig. S7 and Supplementary Information movie). The mixer modules are positioned symmetrically, which feed two mixed media to a channel junction in the middle of the device (which we call the "split junction"; Fig. 1D). Once the mixed media reaches the split junction, the media flows towards the shunt port (S) or down a pair of parallel channels leading to the diffusion chambers (highlighted in red in Fig. 1A and F). The split junction has a separator wall to avoid a diffusive mixing of the two media flows (Fig. 1E). The split junction is also connected to cell outlet ports through serpentine channels (C1 and C2, Fig. 1A). Once cells are loaded in the chip, C1 and C2 ports are closed by small binder clamps on the Tygon tubes just outside of the chip to stop the flows through these ports. The parallel channels act as a source and a sink for diffusion through the rectangular chambers of different lengths. The parallel flows merge downstream of the chambers towards the waste port (W).

At the split junction a laminar flow is created towards the S port (Fig. 1E). Together with a laminar flow at another junction downstream of chamber towards the W port (Fig. 1H), the laminar flow interface serves as an indicator of the balance of the right and left media flows towards the diffusion chambers. The position of the laminar flow interface can be adjusted by fine-tuning the height of the media reservoirs on the hydrostatic pressure controllers thereby equalising the left-right pressure balance. This eliminates the cross-flow across the chambers and enables an establishment of stable diffusion-based chemical gradients.

Computer-controlled gradient of small molecules

First, to test the microfluidic platform, we used fluorescent dyes Sulforhodamine 101 (SR; M.W. = 606.7 Da) and Cascade Blue hydrazide (CB; M.W. = 527.5 Da). We note that SR and CB are relatively small molecules with similar molecular masses. Thus their diffusion coefficients are also similar (estimated values are $413 \mu\text{m}^2 \text{s}^{-1}$ for SR and $437 \mu\text{m}^2 \text{s}^{-1}$ for CB; see Supplementary Information). SR and CB flowed through the left (SR) and right (CB) channels to generate gradients (Fig. 2A).

The fluorescent dyes were supplied as square waves (Fig. 2B and C), which were controlled independently. Fluorescence of CB and SR was quantified by fluorescence microscopy in one of the chambers (300 μm in length). Note that a slight increase in CB fluorescence in the left channels (arrows in Fig. 2B) is due to a bleed-through of SR signal (see Supplementary Information). Fig. 2D and E show the fluorescence along the chamber over time. The gradient of fluorescence is linear for CB while the one for SR is concave. Similar gradients were detected in the other chambers of different lengths (data not shown). If the mass transfer of a chemical occurs only by passive diffusion then it is predicted that at the steady state a linear gradient is established in a rectangular chamber between source and sink channels,²² as observed with CB (Fig. 2D). The most plausible explanation of the concave profile of SR fluorescence is the adsorption of SR on the solid surface of the chamber (Supplementary Information). The detected SR fluorescence is the sum of the signals from the free molecules in solution and those adsorbed on the surface.

Diffusion in the presence of adsorption

The diffusion-adsorption in a chamber can be modelled by Fick's law of diffusion and the law of Langmuir that describes the equilibrium between the molecules in solution and the adsorbing surface³⁴ (see Supplementary Information). This simple model recapitulates the observed fluorescence profiles of SR rather well. Fig. 2F and H show the fluorescence of SR (red) and CB (blue) across the chamber over the 100 s period (10 s interval) after the tracer inputs were switched off (Fig. 2F) or on (Fig. 2H). The observed fluorescence profiles over time are qualitatively similar to the simulation results (Fig. 2G and I). Although SR and CB have similar diffusion coefficients, it took much longer to establish a steady state gradient for SR than CB. Thus, when adsorption occurs, the effective diffusion rate of a molecule can be smaller than predicted by assuming a free diffusion. In this particular experiment with a period of 1200 s, the SR gradient did not reach the steady state profile while the CB gradient did. In most cases, we have no prior knowledge about the adsorption of the molecules of

interest at the solid-liquid interface. Therefore, a fluorescent tracer of a similar molecular weight is not necessarily a good proxy of the molecule to be analysed by gradient generation. If a biochemical of interest interacts with the substrate such as PDMS (for example, retinoic acid³⁵) a careful analysis of gradient dynamics is necessary to interpret experimental results properly. Even so, the steady-state gradient of molecules *in solution* is predicted to be linear and independent of adsorption (Supplementary Information, Fig. S1).

Generation of a gradient of larger molecules

Next, we tested a gradient generation using FITC-dextran (FD; M.W. = 10 kDa) and CB as a reference. The estimated diffusion coefficient of FD is $89.7 \mu\text{m}^2 \text{s}^{-1}$ (Supplementary Information). FD and CB were supplied in square waves (300 s out of sync) to the left (FD) and right (CB) channels (Fig. 3A, upper panel). Note that we detected a significant bleed-through of FD signal in the CB fluorescence (Fig. 3A, arrows in lower panel; see Supplementary Information), which hampers an accurate measurement of CB fluorescence in the presence of FD. Fluorescence was measured in a chamber of length = 500 μm .

Fig. 3D and F show the fluorescence profile across the chamber for every 10 s over the 100 s periods as indicated (grey bars in Fig. 3A). Fig. 3E and G are the corresponding gradients predicted by a passive diffusion without adsorption. The CB gradient in the absence of FD (at $t = 410$ s) was linear (Fig. 3D). By contrast, FD gradients approached a sigmoidal shape after the FD input to the left channel was switched on (Fig. 3D, green curves). The fluorescence intensity profile in the chamber after the input was switched off (Fig. 3F) is similar to the one theoretically predicted (Fig. 3G) except the flatter regions close to the edges of the chamber (black arrows in Fig. 3D, F).

The flatter regions in the concentration profile are also evident in contour plots across the chamber (Fig. 3C, indicated by arrows). These regions were due to inward flow trajectories near the edges (illustrated in Fig. 3B), which creates advection dominated areas. Such advection-dominated areas near the edges of diffusion chambers were reported previously

with FD of M.W. = 40 kDa.²² The estimated flow rate in the parallel channels calculated from the geometry of the device (and the pressures applied to the ports as indicated in Supplementary Information, Table 3) is $\sim 133 \mu\text{m s}^{-1}$. The speed of SR flows measured by capturing time-lapse images of the dye front in the parallel channels was $\sim 88 \mu\text{m s}^{-1}$, which is in good agreement with the estimated flow rate. The speed of inward flows (Fig. 3B), which may affect gradient profiles, should be slower than these values. The flow rate is comparable to the diffusion speed of FD ($89.7 \mu\text{m}^2 \text{s}^{-1}$) but much slower than that of CB ($437 \mu\text{m}^2 \text{s}^{-1}$). This may explain why FD is affected by advection but not CB. Apart from the difference due to the effect of advection, the predicted gradient profiles (Fig. 3E, G) reproduced observed ones (Fig. 3D, F) quite well. The fluorescence profile of CB is little affected by the inward flow, perhaps because its diffusion is fast enough to counteract the effect of the advection.

Dynamic gradient generation

Next, we tested the capability of the microfluidic platform to generate a dynamic gradient. CB media supplied to the left and right channels were controlled independently, so the gradient of varying magnitude, steepness and direction can be generated according to a pre-programmed scheme. Fig. 4 shows an example of a dynamic gradient of CB in a 300 μm chamber in response to trapezoid waves of inputs. Pre-programmed schemes are not restricted to square or trapezoid waves. In fact, any arbitrary function can be adopted to control the input concentration (mixing ratio) of the substances of interest²⁹ to change the magnitude and steepness of the gradient.

Gene expression in budding yeast cells in response to an inducer gradient

We designed the microfluidic device in order to study the behaviour of engineered budding yeast (*S. cerevisiae*) cells in chemical gradients. To test the microfluidic device for bioassays, we cultured yeast cells in the diffusion chambers. The yeast strains harbour a reporter gene encoding a fluorescent protein (Venus, a yellow fluorescent protein), which is expressed in response to a chemical inducer Dox. In the media used for microfluidic experiments (SMM, see Materials and Methods and Supplementary Information), the doubling time of cell growth is 5.4 hours. As cells grow they gradually occupy the entire chamber and those pushed out of the chamber are washed away by the flows in the main channels.

When cells were exposed to Dox uniformly, all cells expressed the reporter fluorescent protein Venus (Fig. S5, at $t = -225$ min). After removing Dox from the chamber, the fluorescence diminished rapidly (Fig. S5, compare $t = -225$ min and 0 min) indicating the reporter gene expression was switched off. When Dox gradient was generated, expression of Venus was observed in a population of cells close to the left channel, i.e. the source of the Dox inducer (Fig. 5A). As the source concentration of Dox increased, the region of expression expanded (Fig. 5A; the positions of the expression boundary with the initial gradient with 0.2-0 $\mu\text{g}/\text{ml}$ of Dox are indicated by red arrowheads). Images throughout the whole experiment are shown in Fig. S5. Dox was supplied with CB as a tracer, which formed a gradient across the chamber with cells (Fig. 5B). Together, these results demonstrate a generation of Dox gradient, which induced a reporter gene expression in yeast cells in a chamber in a concentration-dependent manner.

When source (left) channel concentration of Dox was increased to 1 $\mu\text{g}/\text{ml}$, some cells close to the sink (right) channel started to express the reporter gene (Fig. 5A, at 2670 min, red bracket). This is most likely due to a fraction of Dox diffusing out of the chambers upstream as well as a diffusive mixing at the split junction that separates the left and right flows towards the chambers. The estimated diffusion coefficient of Dox (M.W.= 444.4 Da)

is $470 \mu\text{m}^2\text{s}^{-1}$ which is relatively large; the effect of diffusive mixing may become significant at the highest concentration of Dox. For larger molecules (smaller diffusion coefficient) such as proteins this would not be an issue. To minimise an effect of the diffusive mixing at the split junction, the separation wall that segregates the left and right flows may need to be extended a little longer than the current design.

Conclusions

We have demonstrated the capability of our microfluidic device that can generate highly dynamic diffusion-based gradients. A unique design of the "split junction" in this device allows balancing of the flows in the source and sink channels, thereby eliminating unwanted cross flows in the diffusion chambers that may disrupt gradient profiles and cell-to-cell signaling. Together with the DAW mixer modules, the split junction enables independent, flexible and rapid change of chemical concentrations in the source and sink channels. This dynamic feature, as illustrated in Fig 4, is a distinct advantage of our device design. Unlike the flow-switching device,²² our device is not limited by molecular weights (i.e. diffusion coefficient) for gradient generation.

Our device design, however, has some limitations that include: 1) the steady-state gradient is limited to linear profiles; 2) precise balancing of left and right source/sink flows requires the visualization of the laminar interfaces by fluorescent tracers. This prototype device may also benefit from further design modification to maximise its performance. For example, to minimise the effect of diffusive mixing, the separation wall at the split junction might be extended. On-chip pneumatic valves instead of manual clamping of the tube would simplify the cell-loading process but the advantages need to be weighted carefully against adding an extra layer of complexity.

We also showed that the adsorption of a molecule on the solid surface may greatly affect its gradient profile. Thus, a fluorescent tracer of a similar molecular weight is not always

a good proxy of the molecule to be analysed by gradient generation. As we only used a simple inducible reporter gene expression in yeast (Fig. 5), we have not yet exploited the full capacity of the device for bioassays. We expect this microfluidic device to be a versatile prototype applicable to a broad range of biomedical investigations of cellular response to gradients such as morphogenesis, chemotaxis or axon guidance.

Acknowledgement

We thank Alfonso Jaramillo, Boris Kirov, Marco Thiel and Alessandro De Moura for helpful discussions and advice, Stefan Hoppler and Mamen Romano for critical reading of the manuscript, James Hislop for his help with the plasma cleaner, Alex Brand for the microscopy imaging system and Alistair Robertson for fabricating the hydrostatic flow controllers. We also thank Diane Massie and Yvonne Turnbull for technical assistance. This work was supported by Scottish Universities Life Sciences Alliance (SULSA) and the Principal's Interdisciplinary Fund from the University of Aberdeen.

Supplementary Information

A model of diffusion-based gradient with adsorption

We consider the diffusion of molecules that can be adsorbed on the exposed surface (e.g. PDMS). The process of adsorption can be described by the law of Langmuir.³⁴ The theory of Langmuir assumes that molecules can only be adsorbed on the solid surface that are not yet covered by the molecules. Let ϕ be the fraction of surface already occupied by the molecules. The flux of molecules J_1 being adsorbed by the surface is:

$$J_1 = k_1 u_f (1 - \phi), \quad (1)$$

where k_1 is a rate constant and u_f is the local concentration of the molecule in solution. The backward flux J_2 of the adsorbed molecules from the surface is proportional to ϕ :

$$J_2 = k_2 \phi, \quad (2)$$

where k_2 is another rate constant. We take these fluxes J_1 and J_2 into account to model the diffusion dynamics.

The diffusion term can be described by Fick's second law. The question is how we can combine the law with fluxes J_1 and J_2 . The height (H) of the cell chambers in our microfluidic device is much smaller than the width (W) and length (L, which is parallel to the direction of diffusion); $H = 4.5 \mu m$, $W = 100 \mu m$, $L = 300$ to $700 \mu m$. The characteristic diffusive mixing time (τ) of a substance across the height of the chamber is given by $\tau \sim H^2/D$, where D is a diffusion coefficient. D is typically on the order of 10^{-6} to $10^{-5} cm^2 s^{-1}$ (10^2 to $10^3 \mu m^2 s^{-1}$) in aqueous solution, for which $\tau \sim 0.02$ to 0.2 s. This is orders of magnitude lower than the diffusion time across the length of L or W. We can thus approximate the diffusion with

adsorption by a model in one-dimension described by Eqs. 3-5.

$$\frac{\partial u_f}{\partial t} = D\Delta u_f - J_1 + J_2, -k_d u_f, \quad (3)$$

$$\frac{\partial u_a}{\partial t} = J_1 - J_2, \quad (4)$$

$$\phi = \frac{u_a}{A} \quad (5)$$

where Δ is the Laplacian operator, D is a diffusion coefficient, k_d is the decay (degradation) rate constant, u_a is the local concentration of the adsorbed (immobile) molecule, and A is the maximal u_a (that is, the surface concentration at saturation). At steady state ($t = \infty$), from Eqs. 3 and 4:

$$D\Delta u_f(x, \infty) - k_d u_f = 0, \quad (6)$$

$$J_1 = J_2. \quad (7)$$

From Eqs. 6, the steady state (concentration) gradient *in solution* is independent of adsorption. A steady state solution can be obtained using a boundary condition, which corresponds to the concentration at the left edge ($x = 0$) and the right edge ($x = L$) of a diffusion chamber:

$$u_f(0, t) = C1, \quad u_f(L, t) = C2, \quad (8)$$

where $C1$ and $C2$ are a constant. Assuming $k_d = 0$ (as is the case for fluorescent tracers) and solving Eqs. 6-8, the steady state solution is:

$$\bar{u}_f = C1 + \frac{C2 - C1}{L} x, \quad (9)$$

$$\bar{u}_a = \frac{A \bar{u}_f}{\frac{k_2}{k_1} + \bar{u}_f} \quad (10)$$

$$= \frac{A \bar{u}_f}{\frac{1}{k_a} + \bar{u}_f}, \quad (11)$$

where $\bar{u}_f = u_f(x, \infty)$, $\bar{u}_a = u_a(x, \infty)$; k_a is the adsorption coefficient defined as $k_a = \frac{k_1}{k_2}$ (Fig. S1). Therefore, the steady state gradient *in solution* is linear (and independent of adsorption) in the absence of molecular decay. In the presence of a decay, the gradient is an exponential decay curve. In the presence of adsorption, however, the effective diffusion would be slower than predicted by diffusion coefficient D . For a fluorescent molecule, the total fluorescence is proportional to $\bar{u}_f + \bar{u}_a$, which shows a characteristic concave profile at the steady state (Fig. S1). The gradient of CB's fluorescence is linear while the one for SR is concave, indicating the adsorption of SR on the surface of the chamber.

Cross-bleeding of fluorescence signals

Due to the long tailed excitation spectra of Suoforhodamine 101 (SR) and Fluorescein-dextran (FD), the excitation UV light for Cascade Blue (CB) also excites SR and FD fluorophore. For example, the SR signal bleeding is evident in Fig. S2; the increase of CB signal on the left channel correlates with the rise of SR signal on the same channel (Fig. S2A, arrows) rather than the CB signal on the right channel (Fig. S2A, blue dashed line). Because of this signal bleeding, the steady-state fluorescence profile of CB is altered in the presence of SR (Fig. S2B) or FD.

Estimation of diffusion coefficients

Evans *et al.*³⁶ provides an equation to calculate diffusion coefficients of small molecules from their molecular weights:

$$D = \frac{k_B T \left(\frac{3\alpha}{2} + \frac{1}{1+\alpha} \right)}{6\pi \eta \sqrt[3]{\frac{3 \text{ MW}}{4\pi \rho_{eff} N_A}}}, \quad \alpha = \sqrt[3]{\frac{\text{MW}_s}{\text{MW}}}, \quad (12)$$

where η is the dynamic viscosity of solvent (water), ρ_{eff} is the effective density of a small molecule, k_B is the Boltzmann constant, N_A is the Avogadro number, T is the absolute temperature; MW_s and MW are the molecular weights of the solvent and the molecule for which

we want to estimate the value of D, respectively (the function plotted in Fig. S3A). They showed that calculated coefficients were good estimates of the values determined experimentally.³⁶ To calculate the diffusion coefficient of Sulforhodamine 101 (SR; MW = 606.71 *Da*) and Cascade Blue hydrazide (CB; MW = 527.47 *Da*), we used the following values of constants and parameters: T = 298 K, $\eta = 0.89 \times 10^{-3} \text{ kg m}^{-1} \text{ s}^{-1}$, $\rho_{eff} = 619 \text{ kg m}^{-3}$, $\text{MW}_s = 18 \times 10^{-3} \text{ kg mol}^{-1}$. The estimated values of diffusion coefficients were 413 $\mu\text{m}^2 \text{ s}^{-1}$ for SR and 437 $\mu\text{m}^2 \text{ s}^{-1}$ for CB.

To estimate the diffusion coefficient of FITC-dextran (MW = 10 *kDa*), we used a power law relationship:

$$D = a (\text{MW})^b (\text{cm}^2 \text{ s}^{-1}) \quad (13)$$

with $a = 2.71 \times 10^{-5}$, $b = -0.37$.³⁷ The calculated value of the diffusion coefficient is $8.97 \times 10^{-7} \text{ cm}^2 \text{ s}^{-1} = 89.7 \mu\text{m}^2 \text{ s}^{-1}$.

Decay of gradients in a closed chamber

The flow-switching scheme for gradient generation and maintenance described by Frank and Tay²² operates by alternate opening and closing of the on-chip membrane valves. The valves are open for 1 s each every 2 min, therefore, chambers are isolated from the source and sink channels for ~ 1 min. We calculated how much a gradient diverges from a steady state during this period as they decay by diffusion in a confined environment. This was done by solving the diffusion equation $\frac{\partial u}{\partial t} = D\Delta u$ with a boundary condition:

$$\frac{\partial u}{\partial x} \Big|_{x=0} = \frac{\partial u}{\partial x} \Big|_{x=L} = 0, \quad (14)$$

and an initial condition, which is a linear gradient:

$$u(x, 0) = \frac{Cx}{L}, \quad (15)$$

where C is a constant. In the flow-switching device, L = 1 mm. Fig. S3B shows the plot of the solution for D = 100 and 500 $\mu\text{m}^2 \text{s}^{-1}$ (with C = 1). % error is the fraction of the area diverged from the linear gradient after 60 s, which is plotted against diffusion coefficient in Fig. S3C. For a chamber with L = 1000 μm , D = 208.4 $\mu\text{m}^2 \text{s}^{-1}$ results in 5 % error. From Eq. 12, this corresponds to the molecule weight of \sim 3.5 kDa.

Carbon source for yeast cell growth in microfluidic devices

We found CO₂ production by yeast fermentation disrupts the operation of the platform severely, as the air (CO₂) in any parts of the system make it impossible to control the flow reliably. This limits the duration of an experiment. To circumvent the problem, we tested various carbon sources to replace glucose in the standard synthetic media for yeast growth, which include glycerol (3%), potassium acetate (1%), raffinose (2%) or maltose (2%) (see Material and Methods in the main text). In normal shaking flask cultures, cell growth is slower with raffinose (doubling time = 3.9 hours) than with glucose (2.4 hours). Cell growth with maltose is slower than with those two carbon sources, with doubling time of 5.4 hours. Other than the slower growth, we found no aberrant morphology of cells with these three carbon sources. Cell growth in synthetic media with glycerol or potassium acetate is even slower than that in the maltose media (SMM). We found that yeast cells need to be grown in raffinose media first before being cultured in maltose media; if cells are inoculated into maltose media from a culture of glucose media directly, cells do not grow. This is perhaps because of a catabolite repression in the presence of glucose. Derepression seems to happen in raffinose media, which allows growth with maltose as a sole carbon source. Although raffinose media extends an operation time for microfluidic experiments, fermentation slowly occurred, leading to an appearance of CO₂ bubbles in the system (especially in Tygon tubes). By contrast, maltose completely eliminated this problem with yeast fermentation in microfluidics. We therefore decided to use SMM for microfluidic experiments with yeast cells. The experiment shown in Fig. S5 and S6 (and Fig. 5 in the main text) were performed using

SMM.

We then examined an inducible fluorescent protein expression by a standard Tet-On system illustrated in Fig. S4A. Unexpectedly, we observed a high background expression of the reporter yVenus in the absence of the inducer doxycycline (Dox) when cells were cultured in media with raffinose or maltose (but not in glucose) (Fig. S4B). This makes it difficult to distinguish the induced state from the non-induced state. We therefore adopted an activator/repressor dual system³² illustrated in Fig. S4C. This system suppressed the background expression of the reporter gene in all three media tested in the absence of Dox (Fig. S4D). In SMM (and in raffinose media SMR), 0.1 μ g/ml of Dox was sufficient to induce the expression of yVenus.

Detailed methods for microfluidics

Materials

For media reservoirs connected to M1-M4, W and S ports, 50 ml luer lock syringes were used. For C1 and C2 ports, 20 ml syringes were used. Syringe reservoirs were covered by Parafilm (pierced through by a needle) to avoid contamination. Syringes with media/solutions were connected to Tygon tubes of appropriate lengths through 25Gx5/8" (0.5 mm x 16 mm) needles (Table 1). For S, W, C1 and C2 ports, a short tube was inserted between the chip and the longer tube through needle adaptors. This arrangement allows draining and replacing syringe reservoirs if necessary. The needle adaptors were made by cutting 25Gx5/8" needles by pliers and grinding off edges on a sandstone sharpener. Media/solutions (Table 2) were filter-sterilised (0.2 μ m pore size). The solutions were left in a 30 °C incubator to degas for at least a few hours prior to the experiment. Note that even a tiny air bubble trapped in needles or tubes may disrupt the pressure balance and make flows unsteady. Tubes were connected to syringes, filled with media/solution by gravity flow and clamped at the ends to stop the flow until being connected to a microfluidic chip.

Table 1: Tygon tubes.

Ports	Length ¹
M1-M4	1.3 m
S	1.2 m + 10 cm ²
W	1.2 m + 5 cm ²
C1, C2	0.8 m + 10 cm ²

¹ Use appropriate lengths according to the microscopy system available.

² Short tubes are connected between the longer one and the chip.

Table 2: Media and solutions for microfluidic operation.

Ports/Purpose	Media/Solution	Volume ¹
M1, M3	SMM + 20 μ M CB + 2 μ g/ml Dox	10 ml
M2, M4	SMM	10 ml
Cell loading	SMM	5 ml
Priming/wetting chip	SMM + 0.1% BSA	5 ml
C1, C2, S, W	Water + 0.01% BSA	10 ml

¹ Per port.

Setting up microfluidics

To prepare the device for operation the procedure below was followed (in a laminar air hood to avoid contamination):

1. Affix a microfluidic chip on a solid base (e.g. by Blu-Tack[®]).
2. Draw 5ml SMM+0.1% BSA into 20 ml syringe and attach 25Gx5/8" needle. Remove air from the syringe.
3. Attach a bent needle adaptor to a 10 cm tube and connect the other end to the syringe.
4. Drain the solution out of the tube/needle then insert the needle adaptor to the W port of the chip.
5. Introduce the solution into the chip by gently pushing the plunger. Leave it to flow until all the channels are wet and the solution begins flowing out from the other ports (Fig. S7B).
6. Attach bent needle adaptors to each tube of the syringe reservoirs prepared above and insert them into the ports in the following order: S → C1 → C2 → M2 → M4 → M1 → M3. BSA in the solution for S, C1 and C2 ports (Table 2) blocks the surface to prevent non-specific binding (adsorption) of CB and cells.

At this stage the microfluidic device was set up on the microscope/imaging system as illustrated in Fig. S7A, except the syringe reservoir for the port W (still attached to a syringe used to wet the chip). Syringe reservoirs attached to M1-M4 were set on the hydrostatic controllers and those attached to C1, C2 and S were set up on a separate clamp stand. The chip was kept lower than the syringes all the time to avoid air being introduced inside the chip. The balances of M1/M3 and M2/M4 ports were also adjusted at this point. To do this, tubes adjacent to C1 and C2 ports were clamped first and the syringe reservoir heights were fine-tuned by looking at the laminar flow at the split junction (Fig. 1E).

Loading yeast cells

To load cells into the chip the procedure below was followed:

1. Set the pressure to the ports as indicated in Table 3.
2. Draw cell suspension in SMM + 0.01% BSA into 20 ml syringe, attach 25Gx5/8" needle and remove air. Do not leave cells for long in the syringe.
3. Remove the syringe connected to the port W and let the solution drain. Attach the syringe of cells to the port through 5 cm tube.
4. Clamp tubes adjacent to M1-M4 and S ports to avoid backward flow during cell injection.
5. Inject cells into the chip. Do not push the plunger too hard. It may take several minutes until cells reach the chip.
6. Once enough cells are injected (which flow towards C1 and C2 ports), remove the syringe and replace it with the syringe tube connected to the syringe reservoir with water + 0.01% BSA.
7. Trap cells in the diffusion chambers by changing the heights of C1/C2 syringe reservoirs.
8. Once cells are trapped, level the heights of C1/C2 syringe reservoirs (i.e. almost no flow in cell traps) and adjust their position higher than W syringe reservoir to flush cells at the C1 and C2 ports.
9. Once C1 and C2 ports are (almost) clear of cells, clamp W port to stop flow.
10. Clamp both tubes adjacent to the C1 and C2 ports (clamp a few places to stop flow completely), disconnect the longer tubes at the needle adaptors.
11. Remove clamps of M1-M4 and shunt ports.
12. Remove clamp from waste port to start flow.
13. Set height of syringe reservoirs as suggested in Table 3.
14. Adjust the balance of left and right flows by looking at the laminar flow at the split junction again. Also adjust the balance by looking at loose cells in the chambers by fine-tuning the M1-M4 syringe reservoir heights.

Table 3: Pressure applied to each port.

Operation	Ports	Pressure ¹ (height: <i>cm H₂O</i>)
Cell loading	M1-M4	(closed ²)
	S	(closed ²)
	C1, C2	14
	W	14
Gradient generation (cell culture)	M1-M4	71
	S	37
	C1, C2	(closed ²)
	W	45

¹ Values are for guidance only; different pressure may be applied according to experimental needs.

² Ports are closed by clamping Tygon tubes adjacent to the chip.

Design of split junction

We tested three different designs of the split junction; other parts of the device are identical). One without the flow separation wall was found to be inappropriate for the gradient generation due to an excessive diffusive mixing (data not shown). The overall performances of the other two (Fig. S8) were similar, but the laminar flow at the junction was somewhat easier for observation to balance the flows with the design v10, which has the separation wall (Fig. S8A). We therefore used devices with the split junction v10 most of the time.

Time-lapse movie of flows at the split junction

The movie shows time-lapse images of SR fluorescence at the split junction. The fluorescent dye was supplied as a triangle wave (5 min period \times 2 cycles). Note that the laminar flow interface was not affected as the concentration of SR was altered.

References

(1) Smith, J. C. *Cold Spring Harb Perspect Biol* **2009**, *1*, a002477.

(2) Nahmad, M.; Lander, A. D. *Curr Opin Genet Dev* **2011**, *21*, 726–31.

(3) Rogers, K. W.; Schier, A. F. *Annu Rev Cell Dev Biol* **2011**, *27*, 377–407.

(4) Briscoe, J.; Small, S. *Development* **2015**, *142*, 3996–4009.

(5) Batmanov, K.; Kuttler, C.; Lhoussaine, C.; Saka, Y. *Fundamenta Informaticae* **2012**, *118*, 419–461.

(6) Kim, S.; Kim, H. J.; Jeon, N. L. *Integr Biol (Camb)* **2010**, *2*, 584–603.

(7) Berthier, E.; Beebe, D. J. *Lab Chip* **2014**, *14*, 3241–7.

(8) Lin, B.; Levchenko, A. *Front Bioeng Biotechnol* **2015**, *3*, 39.

(9) Jeon, N. L.; Dertinger, S. K. W.; Chiu, D. T.; Choi, I. S.; Stroock, A. D.; Whitesides, G. M. *Langmuir* **2000**, *16*, 8311–8316.

(10) Irimia, D.; Liu, S.-Y.; Tharp, W. G.; Samadani, A.; Toner, M.; Poznansky, M. C. *Lab Chip* **2006**, *6*, 191–8.

(11) Cooksey, G. A.; Sip, C. G.; Folch, A. *Lab Chip* **2009**, *9*, 417–26.

(12) Millet, L. J.; Stewart, M. E.; Nuzzo, R. G.; Gillette, M. U. *Lab Chip* **2010**, *10*, 1525–35.

(13) Chung, H. H.; Chan, C. K.; Khire, T. S.; Marsh, G. A.; Clark, A., Jr; Waugh, R. E.; McGrath, J. L. *Lab Chip* **2014**, *14*, 2456–68.

(14) Abhyankar, V. V.; Lokuta, M. A.; Huttenlocher, A.; Beebe, D. J. *Lab Chip* **2006**, *6*, 389–93.

(15) Keenan, T. M.; Hsu, C.-H.; Folch, A. *Applied Physics Letters* **2006**, *89*, 114103.

(16) Cheng, S.-Y.; Heilman, S.; Wasserman, M.; Archer, S.; Shuler, M. L.; Wu, M. *Lab Chip* **2007**, *7*, 763–9.

(17) Paliwal, S.; Iglesias, P. A.; Campbell, K.; Hilioti, Z.; Groisman, A.; Levchenko, A. *Nature* **2007**, *446*, 46–51.

(18) Mosadegh, B.; Huang, C.; Park, J. W.; Shin, H. S.; Chung, B. G.; Hwang, S.-K.; Lee, K.-H.; Kim, H. J.; Brody, J.; Jeon, N. L. *Langmuir* **2007**, *23*, 10910–2.

(19) Kim, D.; Lokuta, M. A.; Huttenlocher, A.; Beebe, D. J. *Lab Chip* **2009**, *9*, 1797–800.

(20) Skoge, M.; Adler, M.; Groisman, A.; Levine, H.; Loomis, W. F.; Rappel, W.-J. *Integr Biol (Camb)* **2010**, *2*, 659–68.

(21) Lee, S. S.; Horvath, P.; Pelet, S.; Hegemann, B.; Lee, L. P.; Peter, M. *Integr Biol (Camb)* **2012**, *4*, 381–90.

(22) Frank, T.; Tay, S. *Lab Chip* **2013**, *13*, 1273–81.

(23) Beck, C.; Singh, T.; Farooqi, A.; Venkatesh, T.; Vazquez, M. *J Neurosci Methods* **2016**, *262*, 32–40.

(24) Uzel, S. G. M.; Amadi, O. C.; Pearl, T. M.; Lee, R. T.; So, P. T. C.; Kamm, R. D. *Small* **2016**, *12*, 612–622.

(25) Li Jeon, N.; Baskaran, H.; Dertinger, S. K. W.; Whitesides, G. M.; Van de Water, L.; Toner, M. *Nat Biotechnol* **2002**, *20*, 826–30.

(26) Saadi, W.; Rhee, S. W.; Lin, F.; Vahidi, B.; Chung, B. G.; Jeon, N. L. *Biomed Microdevices* **2007**, *9*, 627–35.

(27) Atencia, J.; Cooksey, G. A.; Locascio, L. E. *Lab Chip* **2012**, *12*, 309–16.

(28) Stroock, A. D.; Dertinger, S. K. W.; Ajdari, A.; Mezić, I.; Stone, H. A.; Whitesides, G. M. *Science* **2002**, *295*, 647–651.

(29) Ferry, M. S.; Razinkov, I. A.; Hasty, J. *Methods Enzymol* **2011**, *497*, 295–372.

(30) Duffy, D. C.; McDonald, J. C.; Schueller, O. J.; Whitesides, G. M. *Anal Chem* **1998**, *70*, 4974–84.

(31) Giuraniuc, C. V.; MacPherson, M.; Saka, Y. *PLoS One* **2013**, *8*, e64419.

(32) Bellí, G.; Garí, E.; Piedrafita, L.; Aldea, M.; Herrero, E. *Nucleic Acids Res* **1998**, *26*, 942–7.

(33) Amberg, D. A.; Burke, D. J.; Strathern, J. N. Methods in yeast genetics: A Cold Spring Harbor Laboratory course manual. 2005.

(34) Tabeling, P. *Introduction to microfluidics*; Oxford University Press: Oxford, U.K., 2005.

(35) Futrega, K.; Yu, J.; Jones, J. W.; Kane, M. A.; Lott, W. B.; Atkinson, K.; Doran, M. R. *Lab Chip* **2016**, *16*, 1473–83.

(36) Evans, R.; Deng, Z.; Rogerson, A. K.; McLachlan, A. S.; Richards, J. J.; Nilsson, M.; Morris, G. A. *Angew Chem Int Ed Engl* **2013**, *52*, 3199–202.

(37) Gribbon, P.; Hardingham, T. E. *Biophys J* **1998**, *75*, 1032–9.

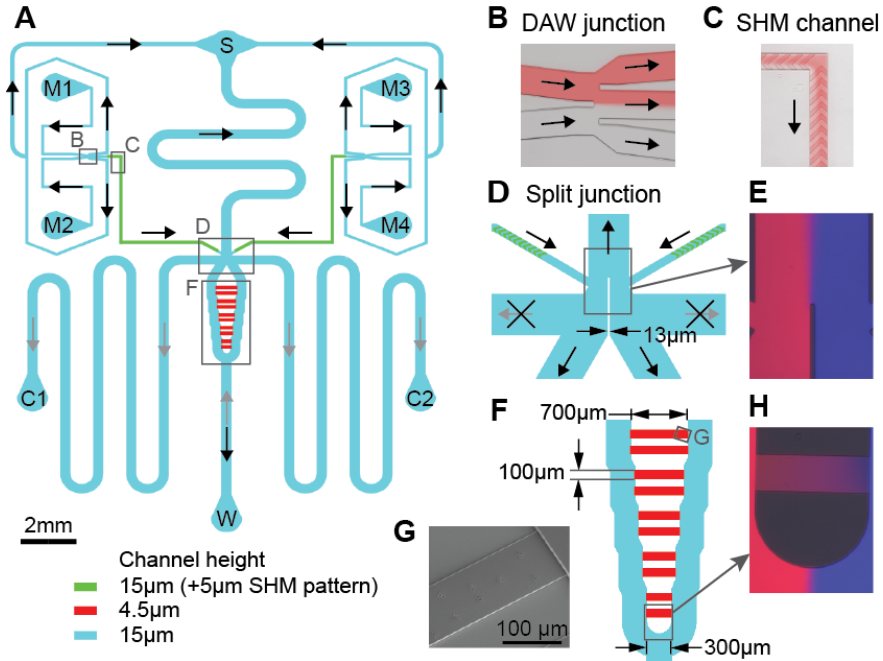


Figure 1: Design of microfluidics. For details, see main text. (A) Overview of the microfluidics. Main channels (light blue), chaotic/staggered herringbone mixer (SHM) channels (green) and cell traps (red) are shown. Black arrows indicate the flow direction for gradient generation and cell culture; grey arrows indicate the flow direction during cell loading. Flows towards ports C1 and C2 are stopped after cell loading. (B) Pseudo-color image of medium flow (Sulforhodamine 101 (SR) in red) at a DAW junction. (C) Medium flow in SHM channel (SR in red). (D) Overview of the split junction. Laminar flow (SR in red; Cascade Blue (CB) in blue) at the junction is shown in E. (F) Overview of the cell traps (red) between a pair of parallel channels. The chambers in the alternative positions have pillars as shown in G (SEM image of a silicon wafer template) for trapping cells. (H) Gradients of two fluorescent tracer dyes (SR, red; CB, blue) in one of the cell traps indicated in F. Note the opposite direction of the gradients.

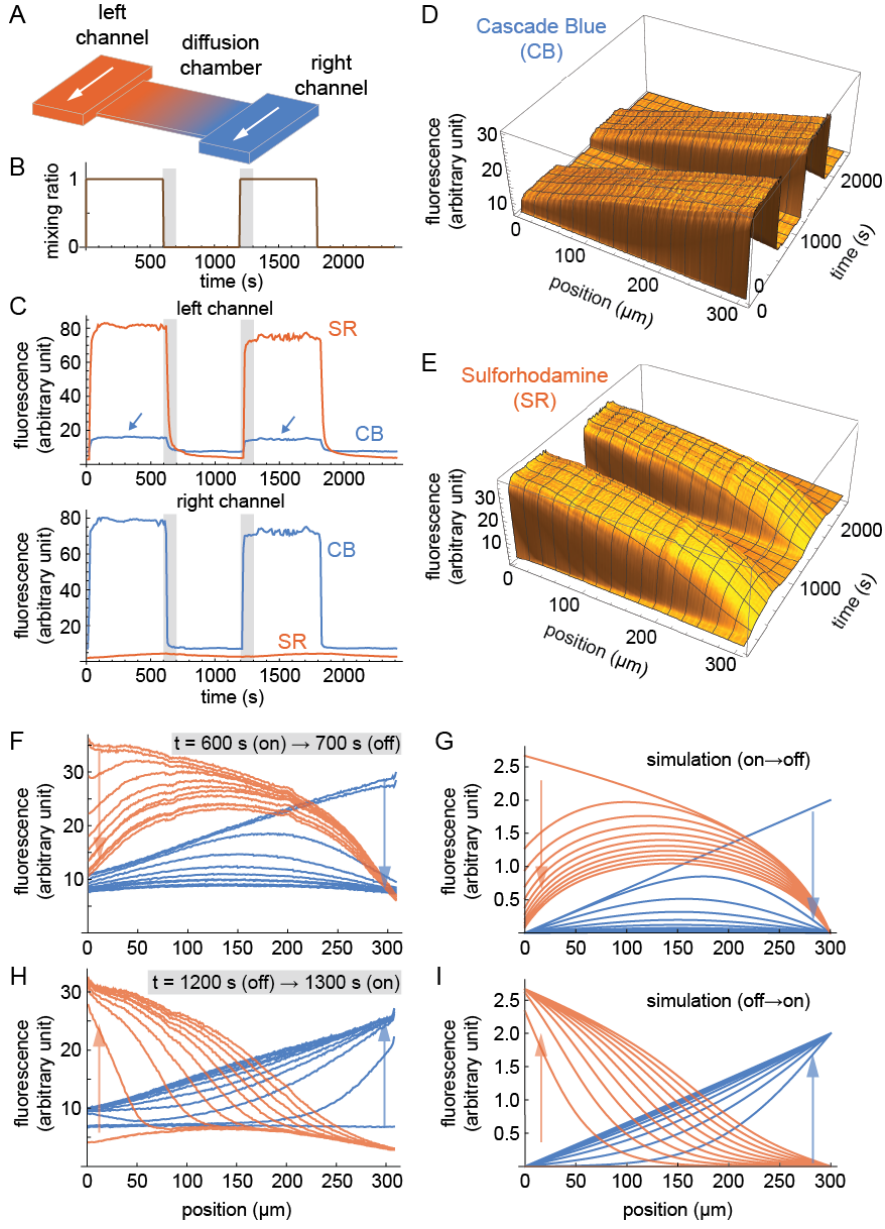


Figure 2: Generation and control of gradients in a diffusion chamber. (A) A schematic of gradient generation by diffusion. (B,C) Fluorescent dyes were supplied in square waves (B) for both channels and their fluorescence was measured in the left (C, upper panel) and right channels (C, lower panel) over time. Arrows in C, upper panel, indicate the fluorescence SR signal bleed-through in the detected CB fluorescence (Supplementary Information). (D,E) The fluorescence intensity measured along the chamber over time. (F, H) Fluorescence across the chamber was measured every 10 s over 100 s periods, which are highlighted as grey bars in B and C. (G,I) Numerical simulations of fluorescence intensity profiles (10 s intervals, over 100 s period) corresponding to the measured ones in F and H, respectively. The direction of the change in gradient profiles are indicated by red or blue arrows in F to I. Parameters: $C_1 = 1$, $C_2 = 0$, $k_a = 5$, $A = 2$ (for SR) or $C_1 = 0$, $C_2 = 2$ (for CB), with diffusion coefficients as mentioned in the text.

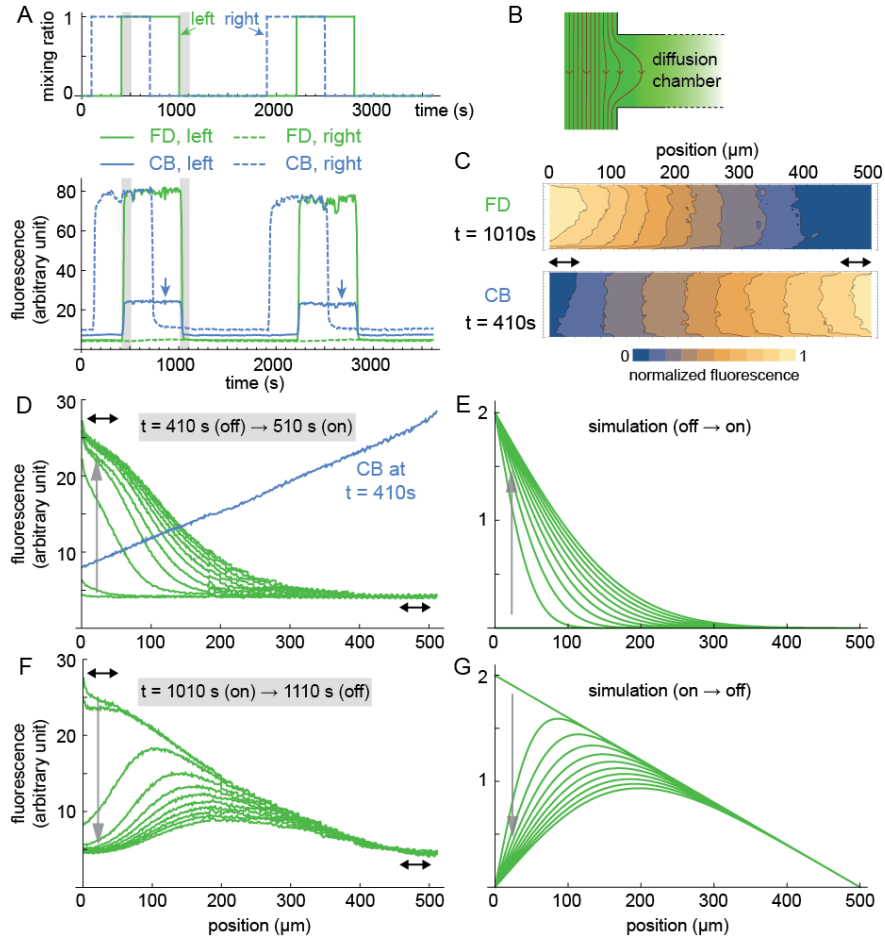


Figure 3: Generation of gradient of FITC-dextran. (A) Fluorescent dyes were supplied in square waves (upper panel; FD in the left and CB in the right channel) and fluorescence in the left and right channels were measured (lower panel). Arrows in the lower panel indicate the bleed-through of FD signal detected as the CB fluorescence. (B) Schematic illustration of inward flow trajectories at the edge of the chamber. (C) Contour plots of fluorescence level across the chamber ($100 \mu\text{m} \times 500 \mu\text{m}$). The advection dominated areas are indicated by black arrows. (D, F) Fluorescence across the chamber was measured every 10 s over 100 s periods highlighted in grey bars in A, and plotted. In D, linear CB gradient at $t = 400$ s is also shown. (E, G) Predicted gradient by diffusion over 100 s period (10 s intervals) after the input is switched on (E) or off (G). The direction of the change in gradient profiles are indicated by grey arrows in D to G. Diffusion coefficient = $89.7 \mu\text{m}^2 \text{s}^{-1}$ was used for the calculation.

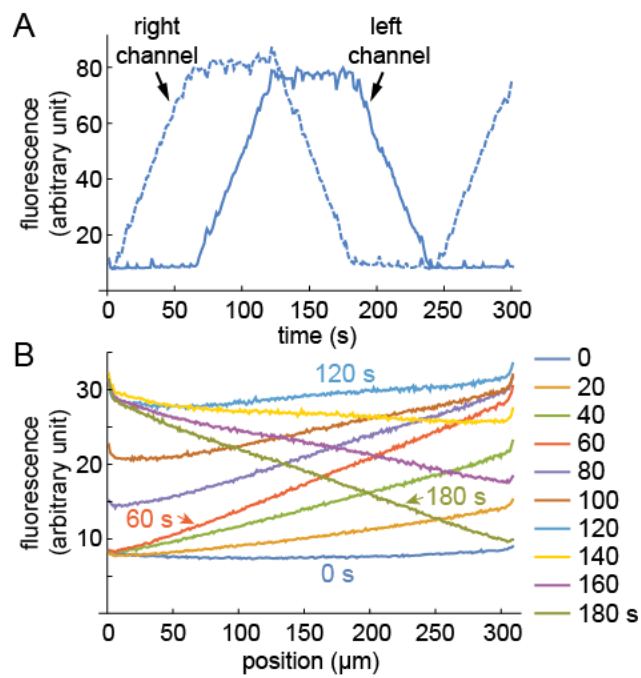


Figure 4: Generation of a dynamic gradient. (A) CB fluorescence in the left and right channels over time. (B) The profile of CB fluorescence across one of the $300\ \mu\text{m}$ chambers at the indicated time points.

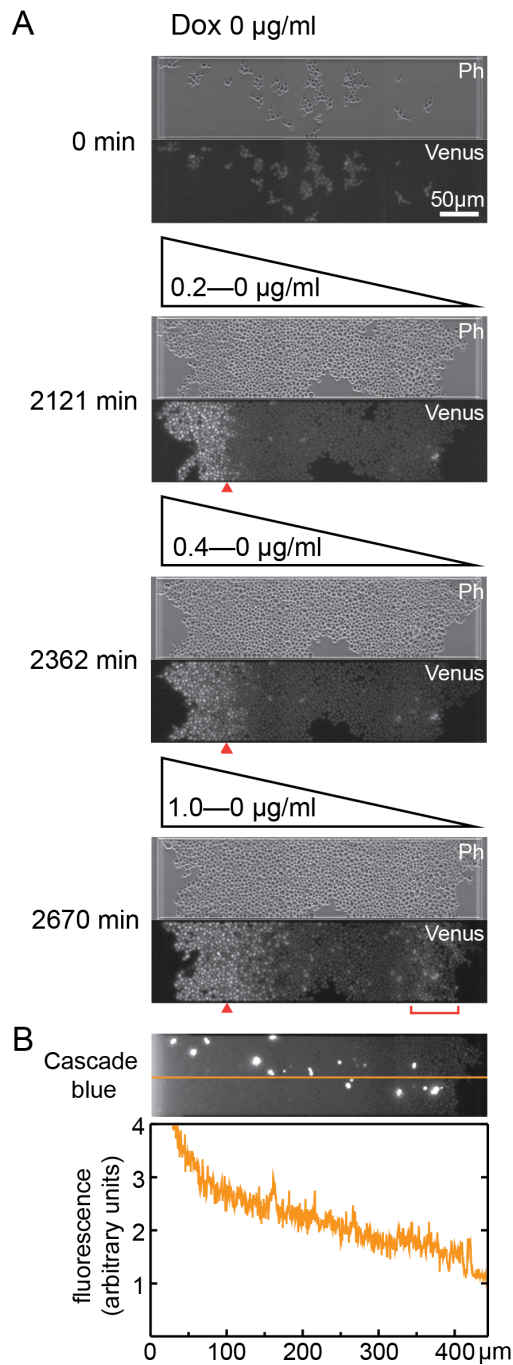


Figure 5: Fluorescent reporter protein expression in yeast in response to the gradient of an inducer. The chamber length is 400 μm . (A) Phase contrast (Ph) and Venus fluorescence images are shown for the indicated time points. Doxycycline (Dox) concentration are also indicated for each image pair. (B) Profile of CB fluorescence on the image (along the yellow line, above) is plotted (bottom). The image was taken at 2670 min. Bright fluorescence indicates dead cells.

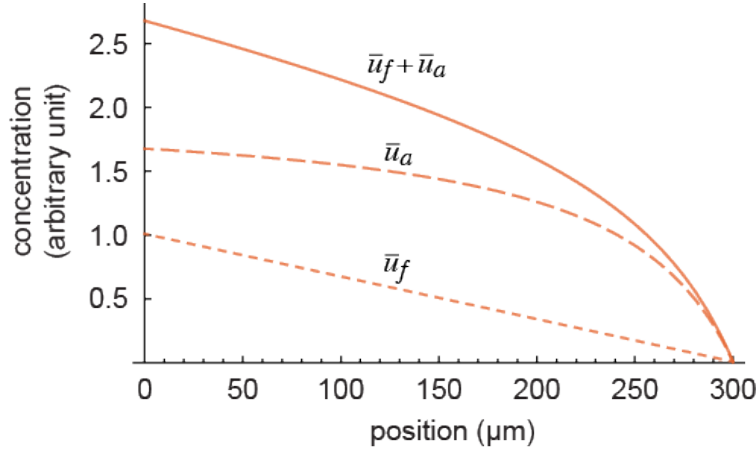


Figure S1: An example of diffusion-based gradient with adsorption at steady state. \bar{u}_f , concentration in solution; \bar{u}_a , concentration of adsorbed molecule. $A = 2, C1 = 1, C2 = 0, k_a = 5, L = 300$ (μm).

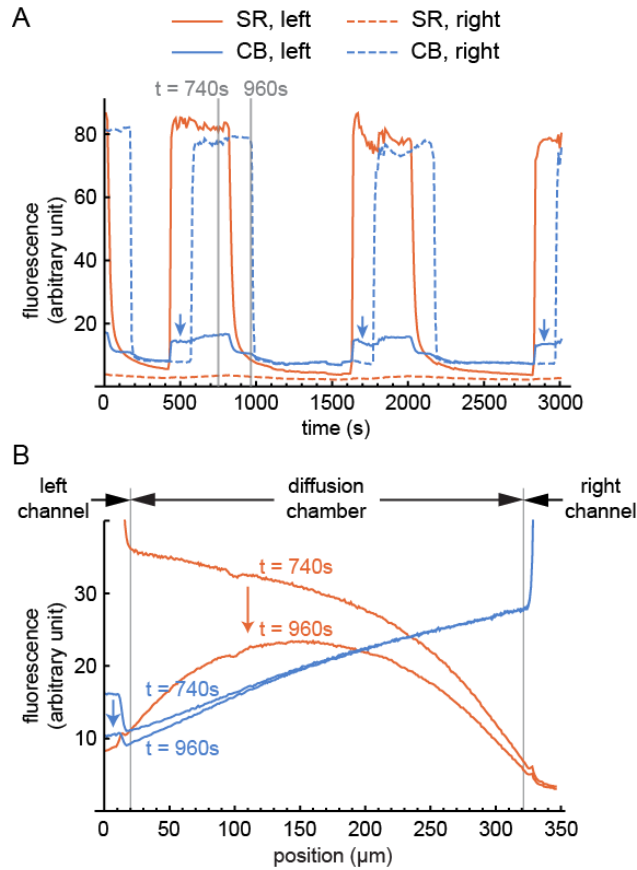


Figure S2: Bleeding of SR fluorescence during CB signal detection. (A) Fluorescence of SR (red) and CB (blue) in the left and right channels over time. Arrows indicate signal bleeding of SR during CB signal detection. (B) Fluorescence profile across the chamber at $t = 740$ s and $t = 960$ s. The fluorescence profile of CB shifted as SR fluorescence decreased, indicating the bleeding of the SR fluorescence.

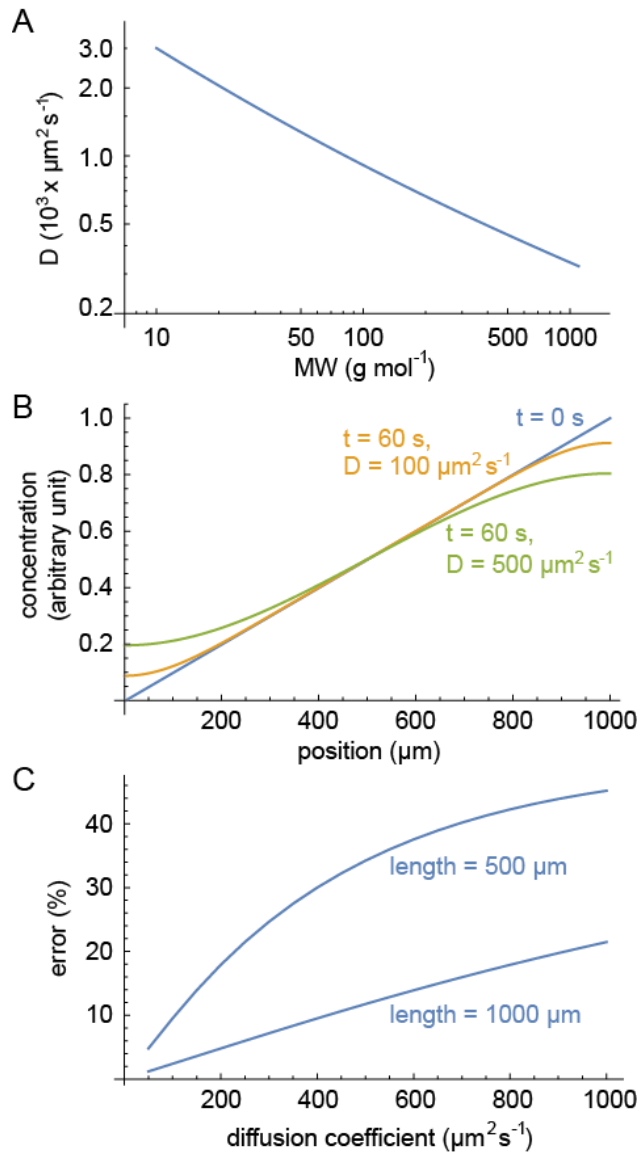


Figure S3: Estimation of diffusion coefficients and error % introduced to the gradient after isolating a chamber from source/sink channels. (A) Diffusion coefficient D is plotted as a function of molecular weight (MW). (B) Gradient decay due to diffusion in a confined chamber of length = $1000 \mu\text{m}$. (C) % error introduced after 60 s in chambers of length = $500 \mu\text{m}$ or $1000 \mu\text{m}$.

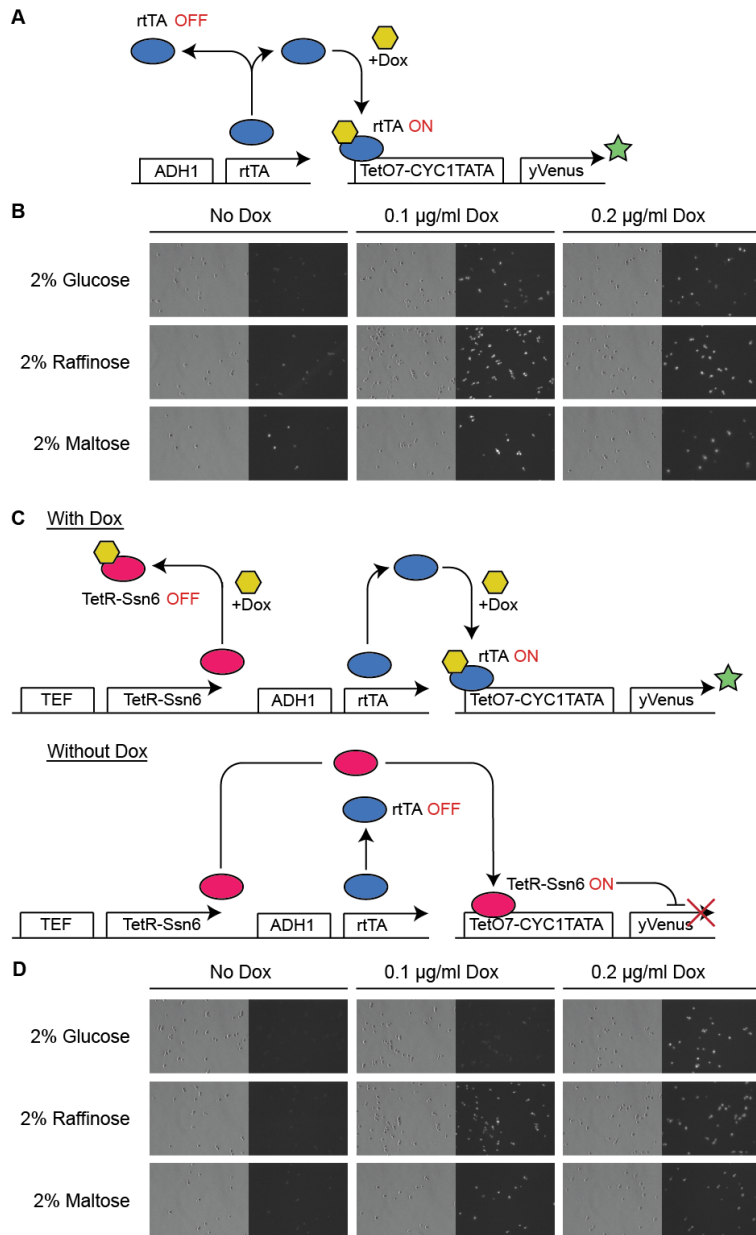


Figure S4: Fluorescent protein reporter expression with various carbon sources. (A, C) Schematics of the inducible expression systems: A, Tet-On system; C, activator/repressor dual system. (B) Expression of yVenus reporter fluorescent protein by the Tet-On system in the absence or presence of doxycycline (Dox). (D) Induction of the reporter gene expression by the dual system in the absence or presence of Dox. Note the background expression of the reporter is suppressed by TetR-Ssn6 in the absence of Dox. In B and D, each pair of panels are phase contrast (left panel) and fluorescence (yVenus, right panel) images. Keys: ADH1 and TEF, constitutively active promoters; rtTA, Dox-inducible transcriptional activator; TetR-Ssn6, a synthetic transcriptional repressor; TetO7-CYC1TATA, the inducible promoter of Tet-On system.

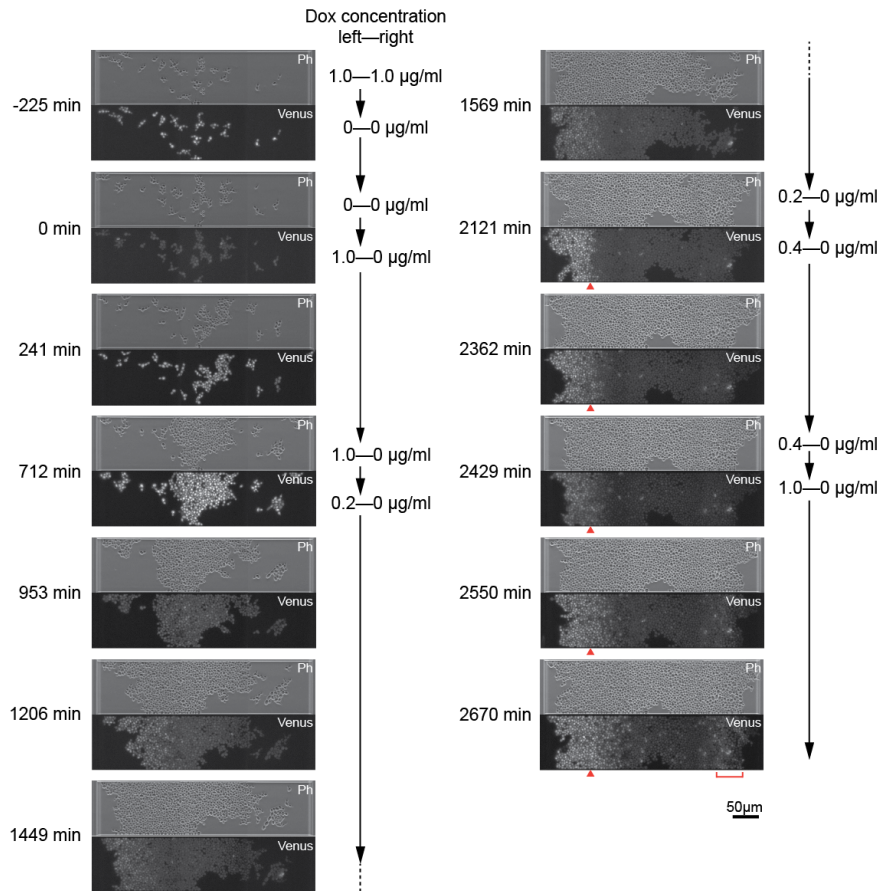


Figure S5: Inducible fluorescent protein reporter expression in yeast cells in a microfluidic chamber. Images (phase contrast (Ph) and Venus) at the indicated time points during the entire course of an experiment are shown. The positions of the expression boundary in the gradient of 0.2-0 $\mu\text{g/ml}$ are indicated by red arrowheads. Fig. 5 in the main text is an abridged version of the images shown here. Dox concentrations in the left and right channels are also indicated.

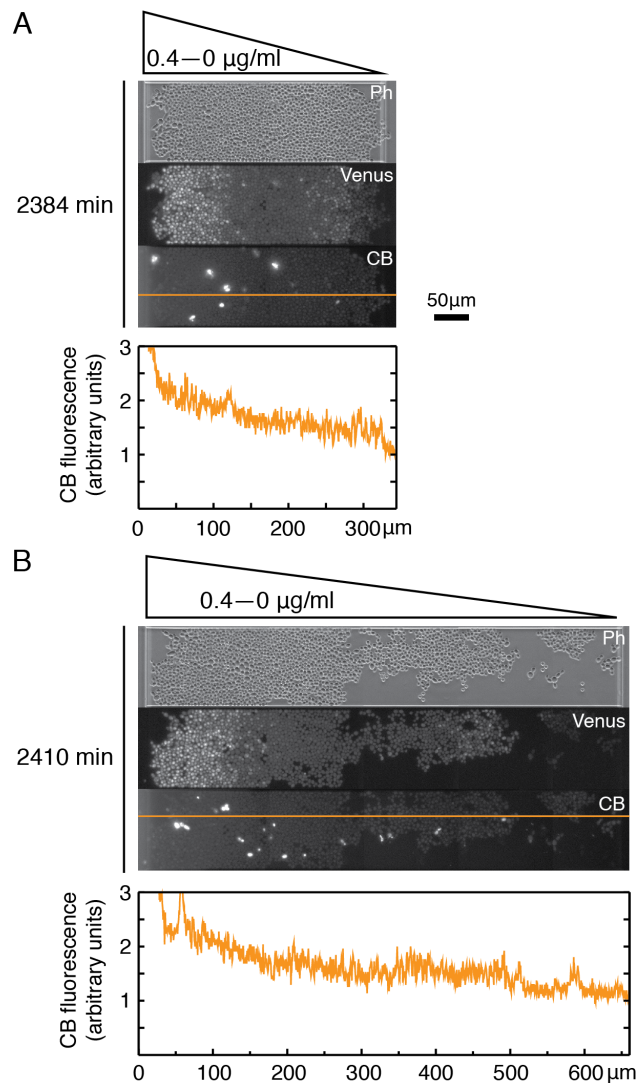


Figure S6: Fluorescent reporter protein expression in yeast in response to the gradient of an inducer. The chamber lengths are 300 μm (A) and 600 μm (B). Phase contrast (Ph), Venus, and CB fluorescence images are shown. Bright fluorescence in the image of CB indicates dead cells. Profiles of CB fluorescence (along the yellow line) are also plotted. The image was taken at the indicated time points (the reference time point 0 min is the same as in Fig. S5).

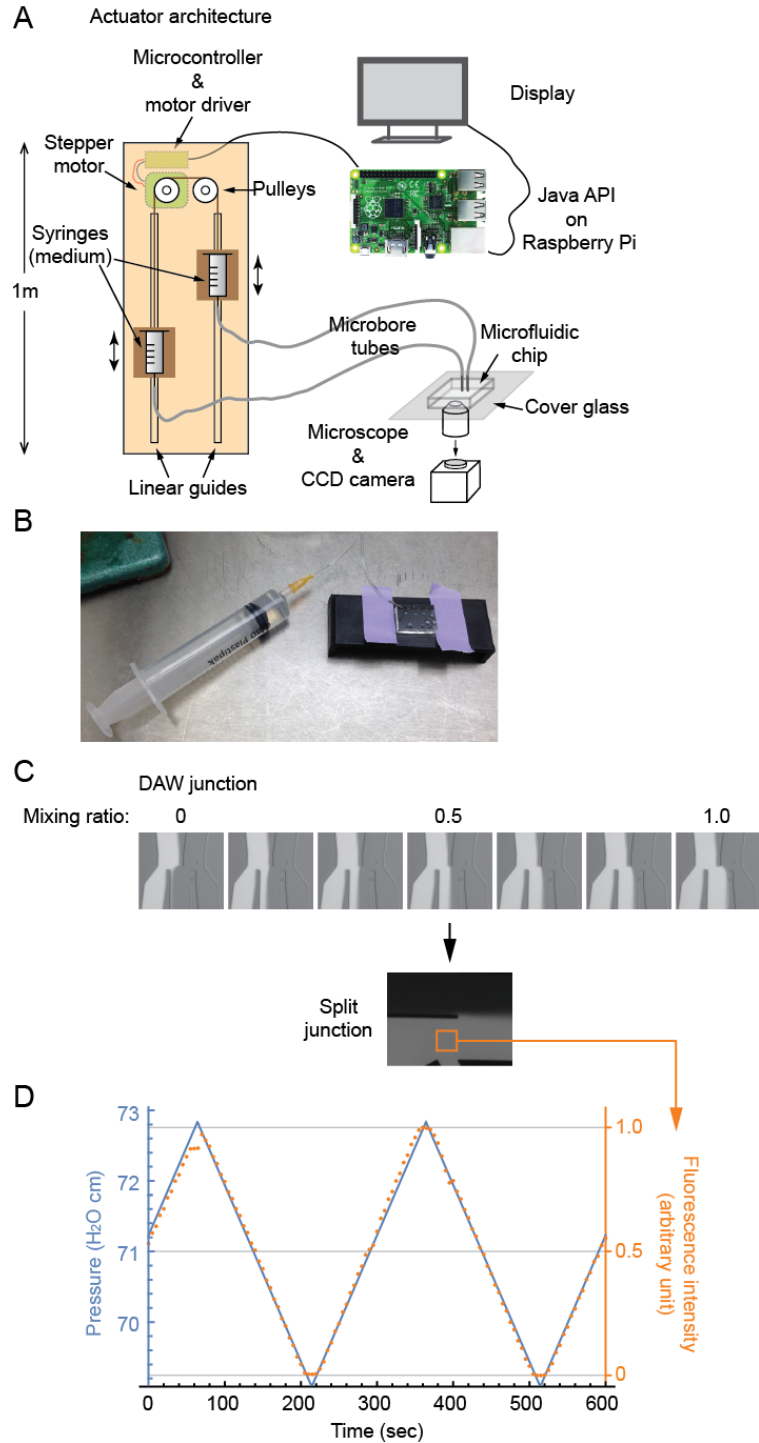


Figure S7: The device setup. (A) Schematic of the system overview. (B) Microfluidic device attached to a syringe for priming/wetting channels. Note the solution flowing out from the ports. (C) Flow of CB at the DAW junction at various mixing ratio. Fluorescence was measured at the rectangular region indicated, and plotted in D (orange dots). (D) The actuator was programmed to produce triangle wave of CB (blue line). The fluorescence intensity fits well to this input over time.

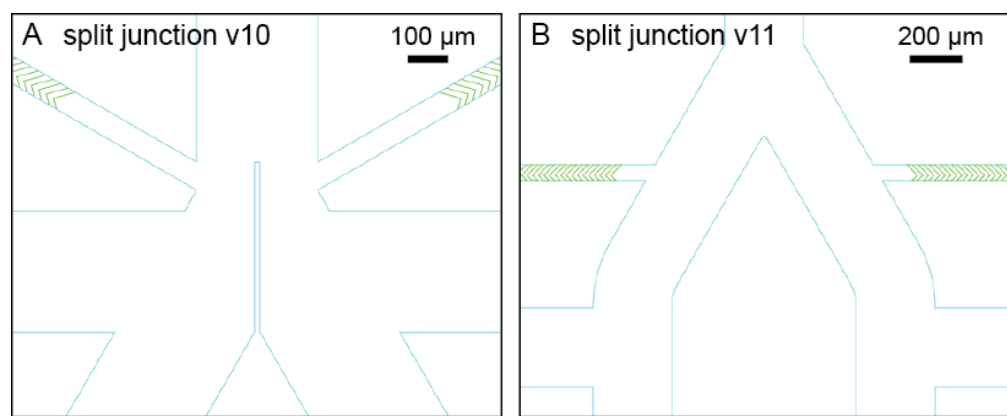


Figure S8: Different designs of the split junction.